




Line-focus solar concentration 10 times higher than the 2D thermodynamic limit

HÅKON J. D. JOHNSEN,^{1,*}  JUAN C. MIÑANO,^{2,3} 
AND JAN TORGENSEN¹

¹Norwegian University of Science and Technology, Department of Mechanical and Industrial Engineering, Richard Birkelands Vei 2b, Trondheim, Norway

²Cedint, Universidad Politécnica de Madrid, 28223 Pozuelo de Alarcón, Madrid, Spain

³Limbak, 28029 Madrid, Spain

*hakon.j.d.johnsen@ntnu.no

Abstract: Line-focus solar concentrators have traditionally been limited by the 2D concentration limit due to the continuous translational symmetry in these systems. This limit is orders of magnitude lower than the 3D limit, severely limiting the achievable concentration ratio compared to point-focus systems. We propose a design principle for line-focus solar concentrators that bypasses this 2D limit, while maintaining a trough-like configuration and only requiring single-axis external solar tracking. This is achieved by combining the concept of étendue squeezing with the concept of tracking integration. To demonstrate the principle, we present a design example that achieves a simulated average yearly efficiency of 80% at a geometric concentration of 335x under light with a ± 9 mrad angular distribution and horizontal single-axis external tracking. We also show how the same design principle can achieve a line-focus with 1563x geometric concentration at 90% efficiency if design constraints are relaxed by foregoing tracking-integration and assuming two-axis external solar tracking. This design principle opens up the design space for high-concentration line-focus solar concentrators, and may contribute to a reconsideration of the trade-off between concentration and acceptance angle in such systems.

© 2022 Optica Publishing Group under the terms of the [Optica Open Access Publishing Agreement](#)

1. Introduction

Line-focus solar concentrators are commonly designed as parabolic trough concentrators or linear Fresnel concentrators. These concentrators require only rotation about one axis to track the sun, and their linear geometry lends itself to being paired with a heat-transfer fluid passing through a receiver tube placed at the focal line. They are designed by taking a two-dimensional concentrator and extruding it in the third dimension to create a line focus [1].

However, a drawback with these line-focus concentrators is their limited concentration ratios. By essentially being two-dimensional concentrators, they are fundamentally limited by the 2D concentration limit of

$$C_{max,2D} = \frac{1}{\sin \theta}, \quad (1)$$

where θ is the acceptance half-angle of the concentrator. This acceptance half-angle must be large enough for the angular radius of the solar disc of 4.7 mrad, convolved with the effect of alignment errors, tracking errors, and surface errors in the concentrator [1].

When evaluating a new type of concentrator, one possible choice is to design for an acceptance half-angle of 9 mrad. This value has been used in some prior work [2,3] and has been adopted in this paper to aid in comparing this principle with those previously proposed design principles. This acceptance half-angle gives a concentration limit of $C_{max,2D} = 111$. Furthermore, because a parabolic mirror falls short of the fundamental limit, commercial parabolic troughs achieve a concentration ratio on the order of approximately 20x to 30x, e.g. the 26x geometric concentration ratio of the commonly used Eurotrough system [4]. It is worth noting that some of the literature

on concentrated solar power gives the geometric concentration ratio of parabolic troughs with reference to the projected area of the receiver tube. That convention would increase these reported concentration values by a factor π . However, throughout this paper, we maintain the convention from nonimaging optics of defining concentration ratio with reference to the surface area of the receiver tube [1], which enables reasonable comparisons to the fundamental concentration limits.

Because both radiative and convective heat losses scale with the exposed surface area of the concentrator, it is desirable to increase this concentration ratio of line-focus concentrators. Several approaches have been proposed to bring the concentration closer to the fundamental 2D limit. This includes aplanatic concentrators [2], compound parabolic concentrators [5], and concentrators designed using the Simultaneous Multiple Surface method [6]. However, these approaches are still limited by the relatively modest value of the 2D concentration limit in Eq. (1).

For comparison, three-dimensional concentrators that concentrate sunlight to a point-focus are fundamentally limited by the three-dimensional concentration limit of

$$C_{max,3D} = \frac{1}{\sin^2 \theta}. \quad (2)$$

At the same acceptance half-angle of $\theta = 9\text{mrad}$, the three-dimensional concentration limit is $C_{max,3D} = 12\,346$ — two orders of magnitude higher than the 2D limit at this acceptance angle. Therefore, a three-dimensional design principle for line-focus concentrators that could bypass the two-dimensional concentration limit would be of interest.

Some earlier approaches to increase the concentration of nominally linear concentrators used a secondary concentrator to split the line-focus into several point-foci or smaller line-foci, where small photovoltaic cells could be placed [7–9]. However, unlike photovoltaic cells, splitting a tubular receiver into many small pieces is not practical. Therefore, we are searching for a concentrator that concentrates light to a continuous unbroken line focus while also utilizing the third dimension to go beyond the 2D concentration limit.

Early approaches to bypass the 2D concentration limit in a continuous line-focus were based on introducing ridges normal to the axis of translational symmetry in such concentrators. However, the overall concentration was relatively low, with acceptance angles suitable for stationary solar concentration [10–12]. The possibility of reaching much higher concentration ratios was, to our knowledge, first shown by Davidson et al. [13]. They used a retro-reflector array and cylindrical lens behind a parabolic trough to boost the concentration ratio, experimentally demonstrating a geometric concentration of approximately 1100x to a line-focus with a reported optical efficiency of approximately 50%. However, this approach required two-axis external solar tracking and a relatively large number of reflections and refractions.

In previous work, we showed that a modified étendue squeezing lens array could be used to achieve line-focus concentration beyond the 2D limit [14], but the concept still required two-axis solar tracking and had an unconventional form-factor with a lens array in front of a trough-like reflector. Here, we show that the concept can be extended to design reflective line-focus concentrators with a form factor more similar to parabolic trough concentrators. Further, we show that it is possible to use tracking integration to eliminate the need for two-axis external tracking. In the remainder of this paper, we introduce a design principle that can be used to design such devices, and present two design examples using the approach.

2. Design principle

Our proposed design principle consists of two steps: First, using étendue squeezing to go beyond the 2D concentration limit, and second using tracking integration to only require single-axis external solar tracking.

2.1. Concentrating beyond the 2D limit

Consider a simple two-dimensional parabolic concentrator. Suppose we require an intercept factor of 1 (all rays from the mirror successfully hit the target) and consider a round target. In that case, the parabolic concentrator achieves a concentration that is a factor π lower than the 2D limit [1]; i.e., at the acceptance half-angle of 9mrad, as considered in this paper, this gives a geometric concentration of $C_g = 35.4$.

In order to increase the concentration closer to the 2D limit, it is possible to replace this parabolic mirror with a two-mirror concentrator. Several approaches can be used to design such concentrators, including the SMS method [15], aplanatic concentrators, or numerical optimization. Such two-mirror concentrators have been shown to increase the concentration ratio closer to the 2D limit, and also have an important additional property that will become important in developing this design approach: They can maintain the high concentration even in off-axis configurations. A simple such two-mirror concentrator designed by an optimization routine is shown in Fig. 1(a).

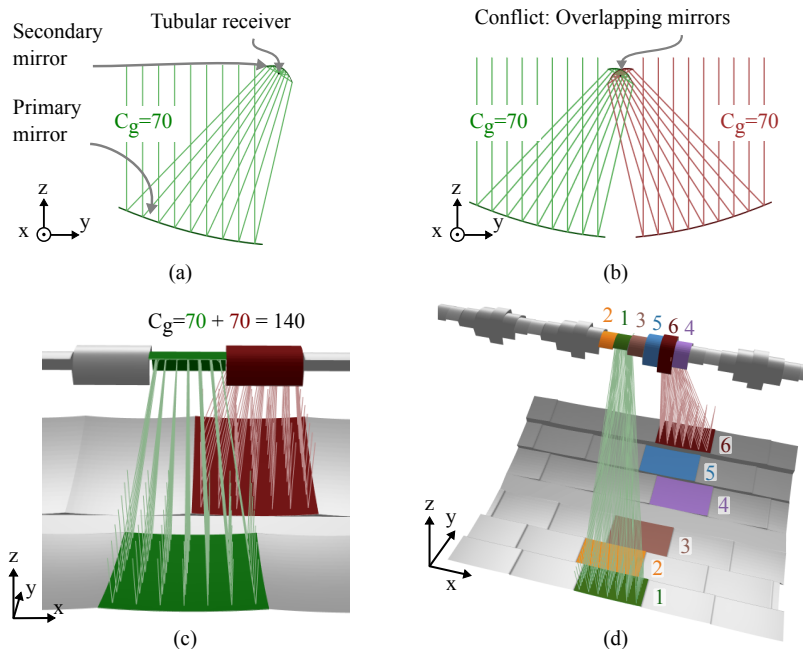


Fig. 1. The design principle can be illustrated as a 4-step process: (a) Start with an off-axis two-mirror concentrator. (b) Add another concentrator aligned to the same tubular receiver. (c) Use the third dimension to resolve the conflict between overlapping secondary mirrors. As shown in gray, the full-length concentrator is made by repeating these off-axis concentrators along the x-axis. (d) Increase the number of off-axis concentrators to increase the concentration ratio further, here shown with six off-axis concentrators in different colors. (Rays are only drawn for off-axis concentrators 2 and 5 to prevent the figure from becoming too cluttered.)

Because the two-mirror concentrators maintain their high concentration in off-axis configurations, a naive approach to increasing the concentration would be to place two such off-axis concentrators next to each other, sharing the same round receiver, as illustrated in Fig. 1(b). In this way, the primary reflector area is doubled, while the receiver area is kept constant. If this were possible, it would effectively double the concentration ratio. Naturally, this approach does not work because the secondary reflectors overlap and block each other. However, let's now

consider that we have another dimension at our disposal. It then becomes possible to resolve this conflict and maintain the high concentration ratio: Each segment of the primary mirror is given some concentrating power along the x-axis, so that they each redirect sunlight to their own segment of the secondary mirror as illustrated in Fig. 1(c).

To further increase the concentration, the number of off-axis concentrators placed next to each other can be increased, as illustrated in Fig. 1(d). Choosing the ideal number of concentrators becomes a matter of optimization: A higher number of concentrators enables higher concentration ratios, but the number must be kept low enough that all the light from each segment of the primary reflector can reach the correct segment of the secondary reflector.

2.2. Terminology of étendue squeezing

The concentrators designed using the principle presented here can be considered to perform what is known as étendue squeezing [16,17], with the number of off-axis concentrators placed next to each other corresponding to the squeeze factor in étendue squeezing terminology. We therefore use the term étendue squeezing concentrator to describe the class of concentrators being proposed. The reader is referred to Ref. [17] for a thorough introduction to the concept of étendue squeezing.

2.3. Tracking integration

A solar concentrator designed using the presented approach requires two-axis solar tracking. Otherwise, the sunlight redirected from one segment of the primary mirror will not hit the correct segment of the secondary mirror. This two-axis tracking is not desirable, as one of the benefits of conventional line-focus solar concentrators is the straightforward solar tracking by simply rotating the concentrator about the optical axis (the x-axis in Fig. 2). To maintain this benefit with the étendue squeezing concentrator, tracking in the longitudinal plane (about the y-axis) can be performed using tracking integration — tracking using relative motions in the concentrator instead of rotating the whole concentrator [18]. In the proposed design principle, tracking integration can be implemented using lateral translation of the secondary reflector. The result is a concentrator where tracking in the transverse plane (about the x-axis) is done using conventional rotation, as illustrated in Fig. 2(a). Then, tracking in the longitudinal plane (about the y-axis) is achieved by translating the secondary mirror along the x-axis without any rotating motion, as illustrated in Fig. 2(b)–2(c).

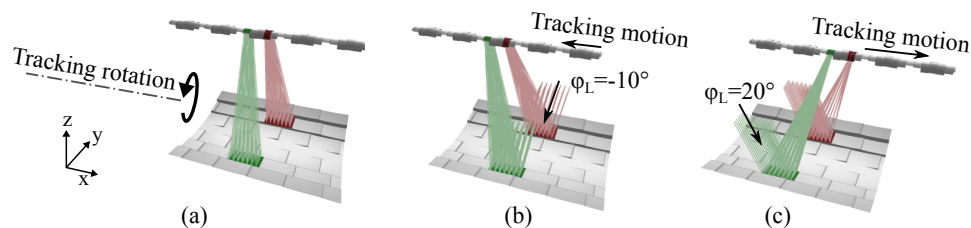


Fig. 2. (a) Tracking in the transverse plane (about the x-axis) is implemented using conventional rotation of the concentrator. (b, c) Tracking in the longitudinal plane (about the y-axis) is implemented using tracking integration, through a lateral translation of the secondary mirror.

From the figure, it may seem like lateral translation distance is relatively large at high angles of incidence. However, because the entire optical design is periodic along the x-axis, the distance of the lateral translation only needs to be the length of this period. (In such a case, the tracking motion would have periodic jumps as it moves from one period to the contiguous one).

3. Design examples

We present two design examples to evaluate the concentration abilities of concentrators designed using the proposed design principle. The first concentrator is designed for optimal performance under horizontal single-axis external tracking, to explore how the full design principle can be used to design real-world concentrators.

As the proposed design principle leads to a new and previously unexplored concentrator geometry, we further explore the limits of this new geometry in a second design example. Here, we remove the support for tracking integration and instead assume two-axis external tracking. This second design example thus explores what concentration ratios are theoretically possible with this concentrator geometry under less stringent constraints of real-world practicality. Both example concentrators are designed using numerical optimization, and the resulting performance is analyzed using numerical ray-tracing.

3.1. Numerical optimization

As a metric to evaluate the proposed design principle, we want to find the maximum concentration that the resulting designs can deliver while maintaining a specific efficiency target. This can be formulated as the following optimization problem:

$$\max f(\mathbf{x}, C_g) = C_g \quad (3)$$

$$\text{such that } \eta(\mathbf{x}, C_g) \geq \eta_{target} \quad (4)$$

where \mathbf{x} is a parametrization of the geometry of the concentrator, and C_g is the geometric concentration ratio.

To implement this objective in the ray-tracing code, we further note that it is possible to directly evaluate the geometric concentration, $C_{g,\eta_{target}}$ that would satisfy the optimization constraint. The resulting objective function is then:

$$\max f(\mathbf{x}) = C_{g,\eta_{target}}(\mathbf{x}), \quad (5)$$

where $C_{g,\eta_{target}}$ is evaluated using the following procedure:

- Sample a set of quasi-random rays across the concentrator aperture area and the $\pm 9\text{mrad}$ top-hat angular distribution, using a low-discrepancy Sobol sequence. For the tracking-integrated concentrator, angle of incidence in the longitudinal plane, ϕ_L , is also used as an additional dimension for this sampling as described in Sec. 3.2.
- Trace the rays through the concentrator represented by the parameters \mathbf{x} .
- Measure the minimum distance from each traced ray to the center of the receiver tube.
- Find the minimum receiver tube radius encircling a fraction η_{target} of the original energy in the traced rays.
- Divide the combined width of the primary concentrators by this receiver tube radius (and a factor 2π) to convert it to an equivalent geometric concentration ratio, $C_{g,\eta_{target}}$.

The design examples were then optimized in three discrete steps, each step using the same objective function given in Eq. (5):

1. The outermost concentrator pair was optimized with a variable squeeze factor to identify a reasonable squeeze factor for further optimization as well as the expected final concentration ratio. This corresponds to optimizing just concentrator pair #1 in Fig. 1(d), with dimensions that leave room for a variable number of other concentrator pairs.

2. An integer squeeze factor N was chosen, and N concentrators were optimized separately for maximum concentration when placed next to each other.
3. The concentrators from step 2 were combined in a complete concentrator model, which was further refined using the objective function in Eq. (5).

Expected surface- and tracking- errors in solar concentrators can be modeled as an apparent increase in size of the solar disc [1]. As a first-order approximation of performance under real-world conditions, we therefore simulated the systems under a solar disc radius of 9mrad, compared to the approximately 4.7mrad angular radius of the actual solar disc.

The systems were modeled in a custom ray-tracer written in Python and accelerated using Numba [19], using a memetic optimization algorithm constructed by combining the Differential Evolution and the SLSQP algorithms from Scipy [20]. The optimization was done on computing resources provided by the NTNU IDUN/EPIC computing cluster [21]. After optimization, concentrators were exported to the commercial optical design software Zemax OpticStudio to verify the simulated performance.

The mirrors were assumed to be perfect reflectors, and the receiver tube was assumed to be a perfect absorber, as these factors are more dependent on material selection than on the optical design. The expected efficiency of a physical implementation must therefore be scaled by the reflectivity of the two mirrors, and by the absorptivity of the receiver. A more refined model may easily consider the angular dependence of both absorptivity and reflectivity.

To prevent concentrators having too impractical aspect ratios, the height of the concentrator (measured from the outermost concentrator segment) was limited not to be higher than the total concentrator width.

These parameters are summarized in Table 1.

Table 1. Design parameters for the two design examples

Condition	Design 1	Design 2
External tracking	Horizontal single-axis tracking	Two-axis tracking
Tracking integration	Yes, in the longitudinal plane	No
Latitude of installation location	30°	-
Target efficiency	$\bar{\eta}_{target} = 80\%$	$\eta_{target} = 90\%$
Surface reflectivity	100%	
Surface quality	Ideal	
Representation of surface geometry	7th order Legendre polynomial	
Maximum aspect ratio (height / width)	1	
Angular extent of simulated sunlight	$\pm 9\text{mrad}$ top-hat distribution	

3.2. Average yearly efficiency

The objective function given in Eq. (5) uses a target efficiency, η_{target} . However, a tracking-integrated concentrator represented by \mathbf{x} and C_g does not have a single efficiency value $\eta(\mathbf{x}, C_g)$. The efficiency varies across the tracking range, and becomes a function of angle of incidence, ϕ_L . We use the notation $\eta_{\phi_L}(\mathbf{x}, C_g, \phi_L)$ to denote this angular dependence.

To get a single efficiency value that can be used during optimization, we use the metric of average yearly efficiency $\bar{\eta}(\mathbf{x}, C_g)$. This has previously been shown to be a useful metric for designing tracking-integrated systems [22,23]. The average yearly efficiency can be defined as a

weighted mean of concentrator efficiency across all angles of incidence:

$$\bar{\eta}(\mathbf{x}, C_g) = \int_{-\pi}^{\pi} e(\phi_L) \times \eta_{\phi_L}(\mathbf{x}, C_g, \phi_L) d\phi_L, \quad (6)$$

where $e(\phi_L)$ is the normalized angular distribution of insolation as intercepted by the concentrator in its expected installation orientation. ϕ_L is the angle of incidence in the longitudinal plane (see Fig. 2), and $\eta_{\phi_L}(\mathbf{x}, C_g, \phi_L)$ is the efficiency of the concentrator under a $\pm 9\text{mrad}$ angular distribution centered at this angle of incidence. Note that with this definition, $\bar{\eta}(\mathbf{x}, C_g)$ does not take cosine projection losses into account [24]. (Under horizontal single-axis tracking as considered in this paper, cosine projections losses are independent of the concentrator design.)

$e(\phi_L)$ can be considered a probability density function of the required tracking angle in the longitudinal plane, and like any probability density function, $\int_{-\pi}^{\pi} e(\phi_L) d\phi_L = 1$.

The computation of the objective function in Eq. (5) is readily extended for the metric of average yearly efficiency by using angle of incidence in the longitudinal plane, ϕ_L , as an additional dimension during the sampling of rays to be traced, with $e(\phi_L)$ as the probability density function.

In our design example, we assume that the concentrator is placed under horizontal single-axis external tracking with a north-south-aligned rotation axis, and we define positive ϕ_L as pointing towards the equator. We then simulate the expected solar irradiation using Meinel and Meinel's air mass attenuation model [25] and, for simplicity assume that cloud cover is not correlated to time of day or time of year. I.e., with the preceding assumption only geometrical and astronomical (and no meteorological) data are necessary for the calculation of $e(\phi_L)$.

The resulting normalized insolation distribution is shown in Fig. 3 for a few different installation latitudes. For the design example in this paper, we used the installation latitude of 30 degrees, meaning that the concentrator will receive sunlight within the angular range of $\phi_{L,min} = -23.5^\circ$ to $\phi_{L,max} = 53.5^\circ$.

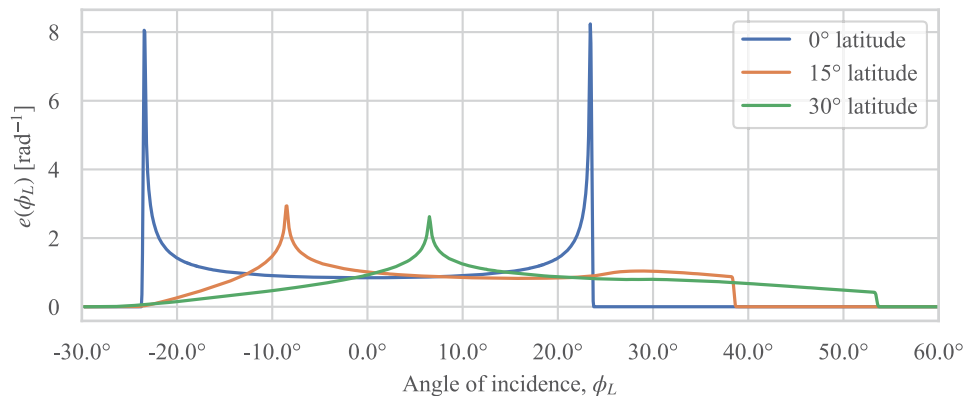


Fig. 3. Normalized distribution of angle of incidence in the longitudinal plane, as seen by a concentrator mounted on a horizontal single-axis external tracker, at different latitudes. At the equator, the distribution varies between approximately $\pm 23.5^\circ$ given by the axial tilt of the earth. At higher latitudes, the distribution spreads out and becomes asymmetrical. In the design example in this work, we assumed a concentrator mounted at a latitude of 30° .

To prioritize concentrating performance over efficiency at the very largest angles of incidence, we specified a target efficiency of $\bar{\eta}_{target} = 80\%$ for Concentrator 1, unlike the $\eta_{target} = 90\%$ used for Concentrator 2 which does not have tracking integration.

4. Results

After optimization, we evaluated the performance of the two optimized concentrators. 3D models of the two concentrators are shown in Fig. 4.

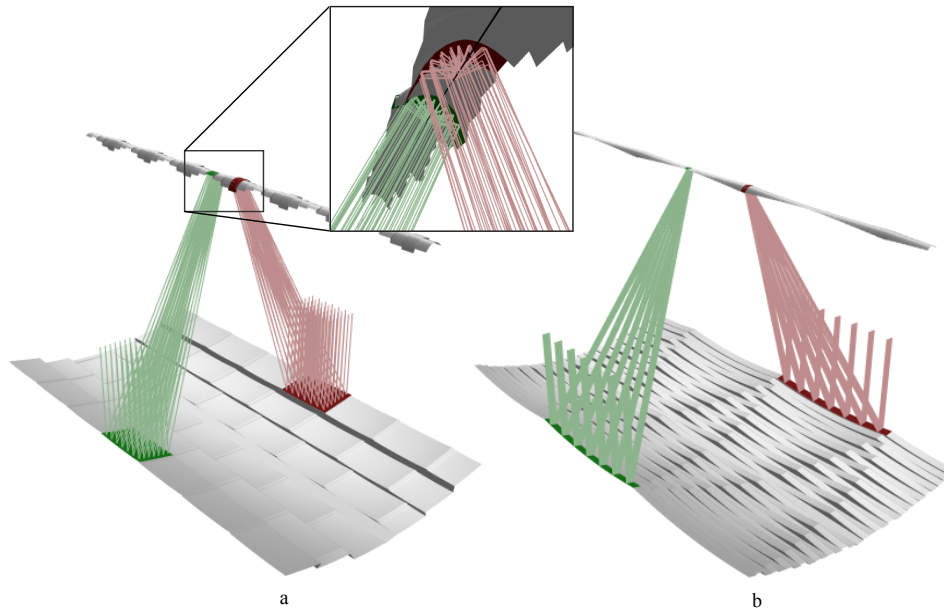


Fig. 4. 3D model of (a) Concentrator 1, with $N = 6$ and $C_g = 335$, (b) Concentrator 2, with $N = 30$ and $C_g = 1563$. In each 3D model, a pair of segments are ray-traced and highlighted in red/green, showing how the segments of the primary mirror redirect the rays to the correct segments on the secondary mirrors. The cutout looks at the secondary mirrors from below, showing how they concentrate the sunlight further towards the receiver tube.

The first design has an optimized geometric concentration of $C_g = 335$ at an average yearly efficiency of $\bar{\eta} = 80\%$ (or $C_g \cdot \pi = 335\pi$ if calculated using the projected area of the receiver tubes as is common in some of the literature on concentrated solar power). This concentration is approximately three times the 2D limit, and almost ten times that of a parabolic trough with the same acceptance angle. This result demonstrates that the proposed design principle can create concentrators with both tracking integration and a very high concentration ratio. The performance of the tracking integration of this concentrator is shown in Fig. 5.

The second design has an optimized geometric concentration of $C_g = 1563$ (or $C_g \cdot \pi = 1563\pi$) at an efficiency of $\eta = 90\%$, more than an order of magnitude higher than the 2D concentration limit. While the lack of tracking integration and requirement for two-axis external tracking makes this second design less practical for real-world applications, it shows that it is possible to design concentrators with extremely high concentration using the proposed design principle.

The efficiency of these concentrators across a span of concentration ratios is shown in Fig. 6(b), showing their performance compared to the 2D limit and to a conventional parabolic trough evaluated under the same $\pm 9\text{mrad}$ angular distribution.

The performance of these example concentrators is compared to the 2D and 3D limits in Fig. 6(b). If the ability to design concentrators above the 2D limit holds at higher acceptance angles, this plot indicates that it might also be possible to design concentrators with more modest concentration ratios and higher acceptance angles.

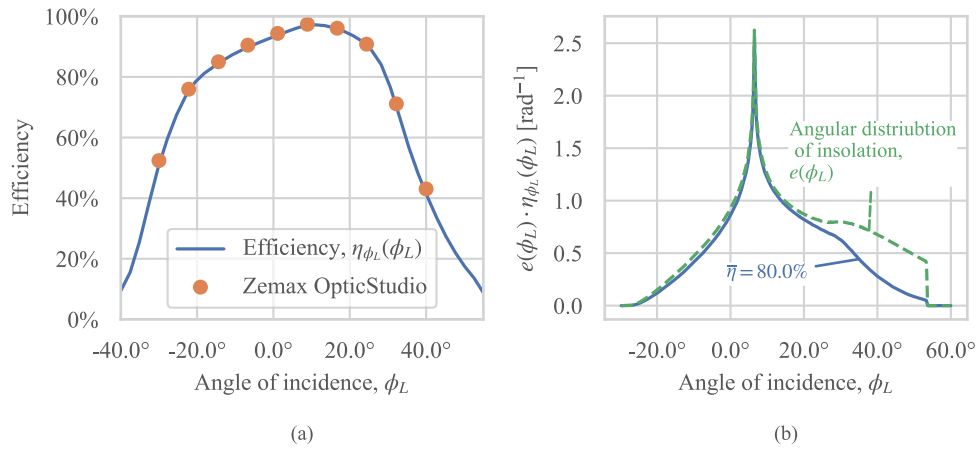


Fig. 5. (a) The efficiency of the tracking integration in Design 1 is asymmetrical across its tracking range in the longitudinal plane, with higher efficiency at positive angles ϕ_L . The optimization algorithm prioritized this because a larger fraction of the yearly insolation is received at these positive angles of incidence. The orange points show simulation results from the commercial ray-tracing software Zemax OpticStudio. (b) The efficiency distribution leads to an average yearly efficiency of 80% under the expected angular distribution of annual insolation, with most of the loss happening at large angles of incidence, corresponding to the winter months.

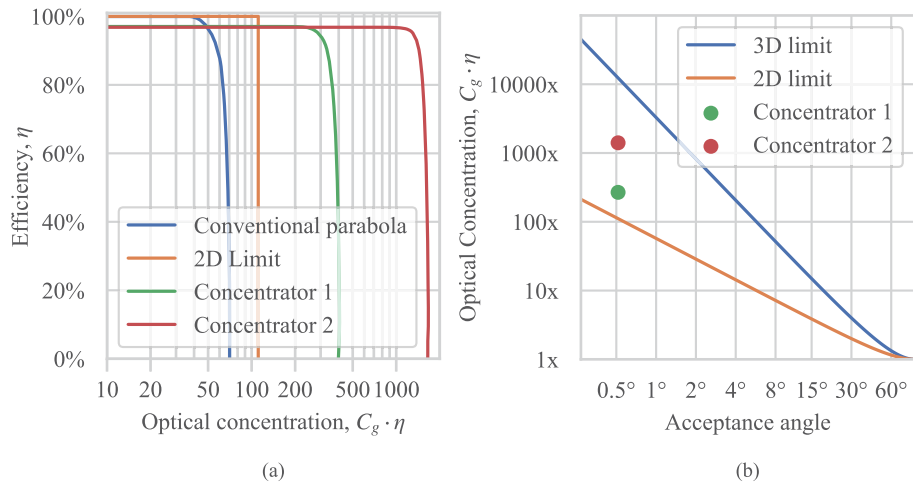


Fig. 6. (a) Efficiency versus concentration on a logarithmic x-axis, showing that both designs outperform the 2D limit when illuminated under a ± 9 mrad angular distribution. For reference, the performance of a conventional parabolic trough with a rim angle of 90° is also included. (b) Concentration limits versus acceptance angle, as given by Eqs. (1) and (2), shown on a log–log scale. (For both the 2D and 3D limit, the efficiency is $\eta = 1.0$)

Both design examples were optimized for light with a top-hat angular distribution of $\pm 9\text{mrad}$. Figure 7 shows the angular acceptance of these concentrators, demonstrating that the optimization algorithm has matched the acceptance angle of the concentrators to this angular distribution.

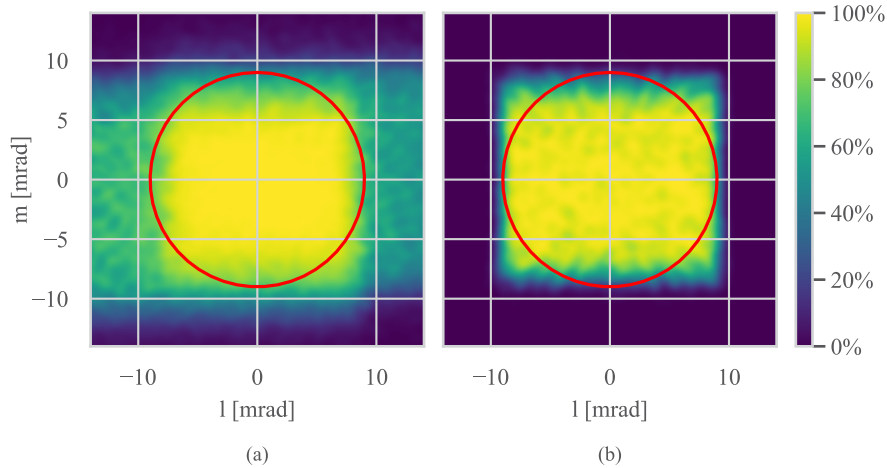


Fig. 7. Concentrator efficiency as a function of incidence angle for (a) Concentrator 1 at a tracking angle of $\phi_L = 0^\circ$, and (b) Concentrator 2. The concentrators are optimized under a $\pm 9\text{mrad}$ angular distribution illustrated by the red circles.

An important factor of consideration for solar concentrators is the homogeneity of the concentrated sunlight. The flux distribution of the example designs is shown in Fig. 8. In the same way as in conventional parabolic trough concentrators, the sunlight is not evenly distributed across the tube. Instead, the majority is concentrated on the upper half of the tube facing the secondary reflector. This indicates that the presented designs are still behind the maximum

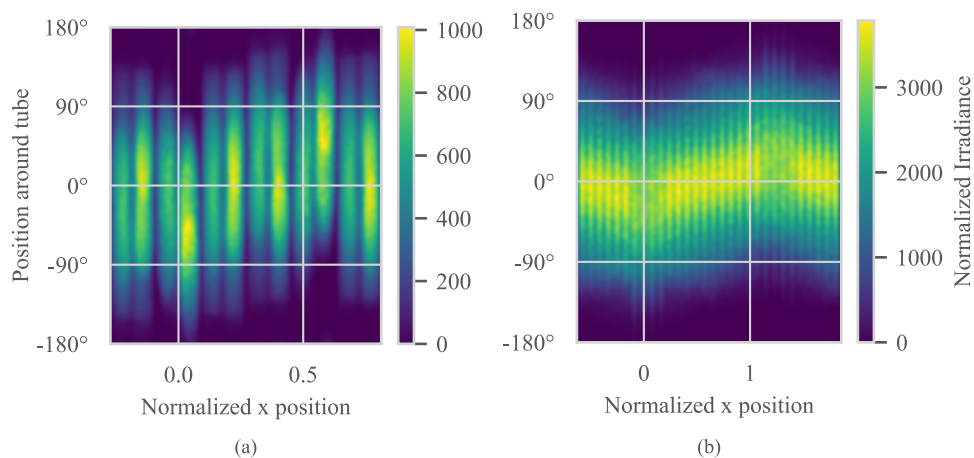


Fig. 8. Irradiance distribution on the surfaces of the receiver tubes of (a) Concentrator 1 at a tracking angle of $\phi_L = 0^\circ$, and (b) Concentrator 2. The irradiance is normalized to 1x solar irradiance, and x-position is normalized to the width of the concentrator. The pattern is repeated along the x-axis for the full length of the solar concentrator. The angular position 0° represents the top of the receiver tube facing the secondary mirror.

concentration achievable by employing this design strategy if the light could be concentrated around the whole surface of the tubes.

The data in Figs. 5–8 comes from the custom Python/Numba-based ray-tracer used during optimization, which is a sequential ray-tracer that considers each mirror segment separately. To confirm that this sequential model is a good representation of the complete concentrator, the systems were also exported to Zemax OpticStudio for a full non-sequential simulation of the whole system. The orange points in Fig. 5(a) come from this simulation, and show good agreement with the Python/Numba-based ray-tracer. The final reported concentration- and efficiency values for Concentrator 2 also comes from the Zemax OpticStudio simulation.

5. Discussion and conclusion

The presented results clearly demonstrate that the proposed design principle can be used to design high-concentration line-focus concentrators. The concentrator with two-axis external tracking demonstrates more than an order of magnitude increase in concentration compared to an ideal two-dimensional concentrator at the same acceptance angle. At the same time, the concentrator with single-axis external tracking shows that it is possible to maintain a very high concentration ratio while modifying the concept so that the concentrator can be mounted on conventional horizontal single-axis solar trackers.

With such a dramatic increase in concentration, the resulting concentration ratios might be higher than what would be practical for a real-world application of the concentrated sunlight. For instance, if the concentrator is 6m wide, the 335 x geometric concentration ratio demonstrated by the first concentrator would correspond to a receiver tube diameter of approximately 5.7mm. This receiver tube would likely be too small for practical alignment and for carrying enough heat transfer fluid to transfer the collected heat. However, we expect the capability to concentrate beyond the 2D limit to also hold for higher acceptance angles. The proposed method might then be used to design concentrators with higher acceptance angles, at more moderate concentration ratios. This would be illustrated by designing concentrators further to the right in Fig. 6(b), and might be an interesting avenue for further research.

Unlike conventional parabolic troughs, concentrators designed using the proposed principle cannot be manufactured by simply bending a reflective sheet of some material. Instead, they must be molded into a three-dimensional shape with several sharp edges. However, some low-cost, high-volume processes might still be applicable for this type of design, for instance, thermoforming of reflective sheets. Additionally, the potential for loosening of manufacturing tolerances in designs with higher acceptance angles might contribute towards a reduction of manufacturing costs.

The concentrators presented as design examples in this paper have a relatively high aspect ratio. They were constrained not to be higher than their width, and the optimization algorithm consistently selected designs at this constraint boundary. This aspect ratio is still much higher than conventional parabolic trough concentrators. Further work may therefore involve exploring how the performance is affected if the aspect ratio is constrained to a lower value.

In summary, we have shown how an étendue squeezing concentrator can be implemented with a form-factor similar to conventional parabolic trough concentrators but with significantly higher concentration, and further showed that tracking integration can be used to allow the resulting concentrator to be mounted on conventional horizontal single-axis external trackers. This way, it is possible to increase concentration ratios while maintaining many of the mechanical and practical benefits of a line-focus system with tubular receivers. We demonstrated the principle by showing a design example achieving a 335 x geometric concentration at 80% average yearly efficiency under horizontal single-axis external tracking. We further showed that even higher concentration ratios are achievable in systems designed without tracking integration, demonstrating a 1563 x

geometric concentration at 90% efficiency. However, this second design example would require a less practical two-axis external tracking.

We believe that the proposed design principle may widen the the design landscape for line-focus solar concentrators, and may contribute to the future development of attractive solar concentrator concepts.

Acknowledgments. Portions of this work were presented at the SolarPACES 2021 Conference, Poster number E-03 [26].

Disclosures. The authors declare no conflicts of interest.

Data availability. Data underlying the results presented in this paper, including Zemax OpticStudio models and data from the figures are available in [Dataset 1](#) [27].

References

1. R. Winston, J. C. Minano, and P. G. Benitez, W. contributions by Narkis Shatz and and John C. Bortz, and W. Bortz, *Nonimaging Optics* (Elsevier Science, 2005).
2. E. T. A. Gomes, N. Fraidenraich, O. C. Vilela, C. A. A. Oliveira, and J. M. Gordon, "Aplanats and analytic modeling of their optical properties for linear solar concentrators with tubular receivers," *Sol. Energy* **191**, 697–706 (2019).
3. L. F. L. de Souza, N. Fraidenraich, C. Tiba, and J. M. Gordon, "Linear aplanatic Fresnel reflector for practical high-performance solar concentration," *Sol. Energy* **222**, 259–268 (2021).
4. M. Geyer, E. Lüpfert, R. Osuna, A. Esteban, W. Schiel, A. Schweitzer, E. Zarza, P. Nava, J. Langenkamp, and E. Mandelberg, "EUROTROUGH - Parabolic Trough Collector Developed for Cost Efficient Solar Power Generation," *Proceedings of the 11th International Symposium on Concentrating Solar Power and Chemical Energy Technologies* p. 7 (2002).
5. M. Collares-Pereira, J. M. Gordon, A. Rabl, and R. Winston, "High concentration two-stage optics for parabolic trough solar collectors with tubular absorber and large rim angle," *Sol. Energy* **47**(6), 457–466 (1991).
6. P. Benítez, R. García, and J. C. Mi nano, "Contactless efficient two-stage solar concentrator for tubular absorber," *Appl. Opt.* **36**(28), 7119–7124 (1997).
7. A. Mohr, T. Roth, and S. W. Glunz, "BICON: High concentration PV using one-axis tracking and silicon concentrator cells," *Prog. Photovolt: Res. Appl.* **14**(7), 663–674 (2006).
8. T. Cooper, G. Ambrosetti, F. Malnati, A. Pedretti, and A. Steinfeld, "Experimental demonstration of high-concentration photovoltaics on a parabolic trough using tracking secondary optics," *Prog. Photovolt: Res. Appl.* **24**(11), 1410–1426 (2016).
9. B. M. Wheelwright, R. Angel, and B. Coughenour, "Freeform lens design to achieve 1000X solar concentration with a parabolic trough reflector," *Proc. SPIE* **9293**, 929316 (2014).
10. M. Rönnelid and B. Karlsson, "Optical acceptance function of modified compound parabolic concentrators with linear corrugated reflectors," *Appl. Opt.* **37**(22), 5222–5226 (1998).
11. J. C. Bortz, N. E. Shatz, and R. Winston, "Performance limitations of translationally symmetric nonimaging devices," *Proc. SPIE* **4446**, 201–220 (2001).
12. J. Nilsson, R. Leutz, and B. Karlsson, "Micro-structured reflector surfaces for a stationary asymmetric parabolic solar concentrator," *Sol. Energy Mater. Sol. Cells* **91**(6), 525–533 (2007).
13. N. Davidson, L. Khaykovich, and E. Hasman, "Anamorphic concentration of solar radiation beyond the one-dimensional thermodynamic limit," *Appl. Opt.* **39**(22), 3963–3967 (2000).
14. H. J. D. Johnsen, A. Aksnes, and J. Torgersen, "Beyond the 2D limit: étendue-squeezing line-focus solar concentrators," *Opt. Lett.* **46**(1), 42–45 (2021).
15. J. Chaves, *Introduction to Nonimaging Optics, Second Edition* (CRC, 2015).
16. P. Benítez, J. Miñano, J. Blen, and F. Garcia, "étendue squeezing optics: Beating the angle-space compromise of symmetrical systems," in *International Nonimaging Optics Workshop*, (2005).
17. P. Benítez, J. C. Miñano, and J. Blen, "Squeezing the Étendue," in *Illumination Engineering*, (John Wiley & Sons, Ltd, 2013), pp. 71–99.
18. H. Apostoleris, M. Stefancich, and M. Chiesa, "Tracking-integrated systems for concentrating photovoltaics," *Nat. Energy* **1**(4), 16018 (2016).
19. S. K. Lam, A. Pitrou, and S. Seibert, "Numba: A LLVM-based Python JIT Compiler," in *Proceedings of the Second Workshop on the LLVM Compiler Infrastructure in HPC*, (ACM, New York, NY, USA, 2015), LLVM '15, pp. 7:1–7:6.
20. P. Virtanen, R. Gommers, T. E. Oliphant, M. Haberland, T. Reddy, D. Cournapeau, E. Burovski, P. Peterson, W. Weckesser, J. Bright, S. J. van der Walt, M. Brett, J. Wilson, K. J. Millman, N. Mayorov, A. R. J. Nelson, E. Jones, R. Kern, E. Larson, C. J. Carey, Í. Polat, Y. Feng, E. W. Moore, J. VanderPlas, D. Laxalde, J. Perktold, R. Cimrman, I. Henriksen, E. A. Quintero, C. R. Harris, A. M. Archibald, A. H. Ribeiro, F. Pedregosa, and P. van Mulbregt, and S. Contributors, "SciPy 1.0: Fundamental algorithms for scientific computing in Python," *Nat. Methods* **17**(3), 261–272 (2020).
21. M. Sjalander, M. Jahre, G. Tufte, and N. Reissmann, "EPIC: An Energy-Efficient, High-Performance GPGPU Computing Research Infrastructure," arXiv:1912.05848 [cs] (2021).

22. H. J. D. Johnsen, A. Aksnes, and J. Torgersen, "High-performance stationary solar tracking through multi-objective optimization of beam-steering lens arrays," *Opt. Express* **28**(14), 20503–20522 (2020).
23. A. Ito, D. Sato, and N. Yamada, "Optical design and demonstration of microtracking CPV module with bi-convex aspheric lens array," *Opt. Express* **26**(18), A879–A891 (2018).
24. K. Lovegrove and W. Stein, *Concentrating Solar Power Technology: Principles, Developments, and Applications*, Woodhead Publishing Series in Energy (Woodhead Publishing, 2021).
25. A. B. Meinel and M. P. Meinel, *Applied Solar Energy: An Introduction* (Addison-Wesley, 1976).
26. H. J. D. Johnsen, J. C. Miñano, and J. Torgersen, "Towards a High-Concentration Line-Focus Concentrator: Étendue-Squeezing and Tracking Integration," Presented at *SolarPACES 2021*, Online, 27. Sept - 1. Oct. 2021.
27. H. J. D. Johnsen, J. C. Miñano, and J. Torgersen, "Supplemental Data for Line-focus solar concentration 10 times higher than the 2D thermodynamic limit," figshare (2022) <https://doi.org/10.6084/m9.figshare.19228254>.